Rotational-state-changing collisions between N_2^+ and Rb at low energies

A. D. Dörfler
Department of Chemistry, University of Basel, Klingelbergstrasse 80, 4056 Basel, Switzerland

E. Yurtsever
Department of Chemistry, Koç University, Rumelifeneriyolu, Sariyer, TR-34450, Istanbul, Turkey

P. Villarreal and T. González-Lezana
Instituto de Física Fundamental IFF-CSIC, Consejo Superior de Investigaciones Científicas, Serrano 123, E-28006 Madrid, Spain

F. A. Gianturco[*]
Institut für Ionen Physik und Angewandte Physik, Leopold Franzens-Universität, Technikerstrasse 25, A-6020, Innsbruck, Austria

S. Willitsch[†]
Department of Chemistry, University of Basel, Klingelbergstrasse 80, 4056 Basel, Switzerland

We present a theoretical study of rotationally elastic and inelastic collisions between molecular nitrogen ions and Rb atoms in the sub-Kelvin temperature regime prevalent in ion-atom hybrid trapping experiments. The cross sections for rotational excitation and de-excitation collisions were calculated using quantum-scattering methods on *ab initio* potential energy surfaces for the energetically lowest singlet electronic channel of the system. We find that the rotationally inelastic collision rates are at least an order of magnitude smaller than the charge-exchange rates found in this system, rendering inelastic processes a minor channel under the conditions of typical hybrid trapping experiments.

I. INTRODUCTION

Over the past ten years, the development of methods for the simultaneous confinement of ultracold atoms and ions has progressed rapidly, enabling the exploration of interactions between charged and neutral particles in the sub-Kelvin temperature regime [1–5]. Typical "hybrid" trapping experiments combine radiofrequency ion traps for the trapping and cooling of atomic and molecular ions [6] with magnetooptical [7–11], magnetic [12], or optical [13–15] traps for the confinement of ultracold atoms, typically alkali or alkaline earth species such as Rb, Ca, or Li. Early studies focused on elastic, inelastic, and reactive collisions between atomic ions and neutral atoms and uncovered an astonishingly rich and diverse chemistry for these seemingly simple diatomic collision systems. Light-assisted processes in electronically excited collision channels were found to play a major role in many systems [8,16], with nonadiabatic and radiative charge exchange as well as radiative association constituting dominant processes [17]. These reactions usually compete with elastic and inelastic collisions [18–20] which change the kinetic and internal energies of the scattering partners, but leave their chemical identity intact.

Most recently, a new focal area has developed in the field which introduces molecular ions into hybrid experiments to study interactions between cold molecular ions and neutral atoms [21–24]. The increased complexity of these collision systems opens up possibilities for more complex collision dynamics [24] and for additional reactive processes involving the formation and breaking of chemical bonds [25] which often compete with one another. The present article is the fourth in a series of a combined experimental and theoretical study aimed at exploring the role and competition of different collisional processes in the prototypical N_2^+ + Rb system in the cold regime. While our previous reports focused on radiative association [26] and nonadiabatic charge exchange [21,24] in this system, the present study theoretically investigates the role of rotationally inelastic collisions using quantum scattering calculations on *ab initio* potential energy surfaces (PES).

As the main result of the present study, we find that the rate coefficients for rotationally inelastic collisions are at least an order of magnitude smaller than those for nonadiabatic charge exchange established in Ref. [24] at the collision energies relevant for hybrid trapping experiments. One can therefore conclude that inelastic processes play only a minor role under typical experimental conditions. The implications of the present findings for other cold molecular-ion alkali-atom collision systems are also discussed.

_____

[*]francesco.gianturco@uibk.ac.at
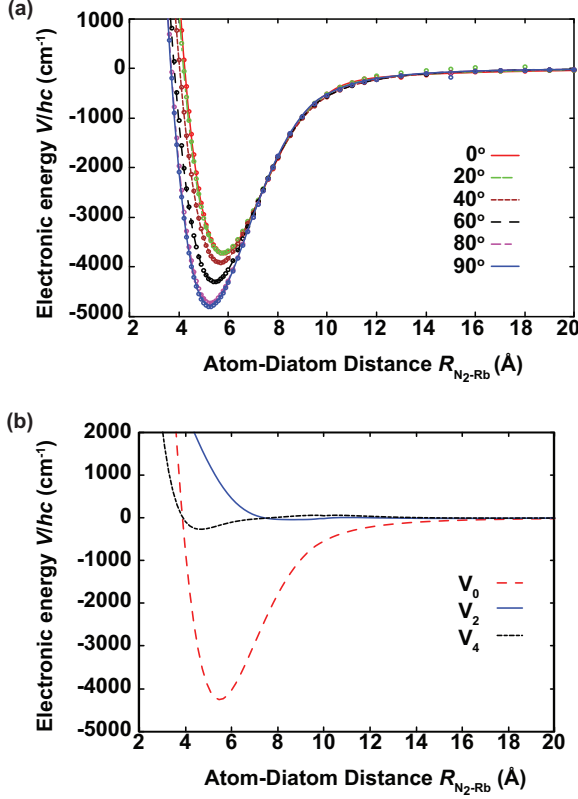[†]stefan.willitsch@unibas.ch

FIG. 1. (a) One-dimensional cuts of the PES of the singlet channel of the N_2^+ ($^2\Sigma_g^+$) + Rb($5s\,^2S_{1/2}$) collision system as a function of the N_2^+-Rb distance R for different orientation angles θ. The symbols represent the *ab initio* points, lines correspond to fits of the *ab initio* data to a Legendre expansion up to fourth order. (b) Radial expansion coefficients V_λ, $\lambda = 0, 2, 4$, of the Legendre expansion of the PES in (a) as a function of R. See text for details.

II. COMPUTATIONAL METHODS

A. Potential energy surface

The potential-energy surface (PES) used in the present scattering calculations is the same as in our previous study [26], where details of the relevant computational methods can be found. Figure 1(a) shows one-dimensional cuts through the PES of the lowest singlet collision channel from Ref. [26] as a function of the N_2^+-Rb distance R at different N_2^+-Rb orientation angles θ with the N-N bond length fixed at its equilibrium value of $r = 1.178$ Å.

To prepare the PES as input for the multichannel quantum scattering calculations outlined below, we fitted the *ab initio* points in Fig. 1(a) to a Legendre expansion up to fourth order [26]:

$$V(R, \theta) = \sum_{\lambda=0}^{\lambda_{\max}} V_\lambda(R) P_\lambda(\cos\theta). \qquad (1)$$

Here, R is the distance between the centers-of-mass of the collision partners and θ is their orientation angle, while $P_\lambda(\cos\theta)$ are Legendre polynomials. The expansion coefficients $V_\lambda(R)$ describe the relative strength of the anisotropy of each multipolar term. Because N_2^+ is a homonuclear diatomic molecular ion, only even terms in λ occur. The anomalous point in the

potential cut of $\theta = 90°$ around $R_{N_2-Rb} = 15$ Å is likely due to the highly nonlinear behavior of the multiconfigurational self-consistent field (MCSCF) equations underlying the *ab initio* calculations [26] when there are several interacting states present. However, the deviation of just one point is of minor importance with respect to reproducing the correct asymptotic behavior of the potential in the fits [see Fig. 1(a)].

Figure 1(b) shows the dominant V_λ coefficients with $\lambda = 0, 2, 4$. Higher-order terms are not depicted because their contributions are shielded by the steep repulsive potential generated by the $\lambda = 2$ term below $R = 4$ Å. The term with $\lambda = 0$ corresponds to the isotropic polarizability α_0 of the potential, the $\lambda = 2$ term represents the dipolar polarizability α_2. Together they describe the polarizability as $\alpha_0 P_0 + \alpha_2 P_2(\cos\theta)$. Both terms scale with R^{-4} for $R \to \infty$. The interaction between the molecular ion and the interacting Rb atom is therefore described by the anisotropic forces at short distances up to the repulsive wall and by the attractive long-range forces caused by the molecular charge polarizing the impinging atom. The anisotropy of the interaction which is represented by the $\lambda = 2, 4$ terms is the driving force for rotationally inelastic collisions.

Within the interval 2.5 Å $\leqslant R \leqslant$ 20 Å, the potential curves of Fig. 1 were fitted to the expansions

$$V(R, \theta) = \begin{cases} \sum_{n=0}^{6} p_n(\theta) \exp[-n\alpha(\theta)(R - R_0(\theta))], & R \leqslant R_c, \\ \sum_{n=4}^{8} \dfrac{C_n(\theta)}{R^n}, & R > R_c, \end{cases}$$
$$(2)$$

where the $p_n(\theta)$ are expansion coefficients, $R_0(\theta)$ is a fit parameter approximating the position of the minimum of the potential at a given orientation angle θ, and the $C_n(\theta)$ are the long-range multipolar coefficients. The matching point of the two expansions was chosen at $R_c = 10$ Å. At this point, the long-range potential already behaves properly at long distances, i.e., the leading term of the long-range interaction is of the form $-1/R^4$.

From the averaged value $C_4 = [C_4(0°) + 2C_4(90°)]/3$, we obtained the isotropic dipole polarizability of Rb, $\alpha_{Rb}^0 = -2C_4 \approx 46.7$ Å^3. This value is close to the experimental result for isolated Rb atoms ($\alpha_0 = 48.7$ Å^3 [27]).

The radial coefficients up to fourth order were obtained from a collocation procedure considering the potential curves at $\theta = 0, 40,$ and $90°$ to obtain the first three coefficients $V_0(R)$, $V_2(R)$, and $V_4(R)$ of the expansion Eq. (1):

$$V_0(R) = V(R, 0°) - V_2(R) - V_4(R),$$
$$V_2(R) = [0.694\,V(R, 0°) + 0.625\,V(R, 40°)$$
$$- 1.319\,V(R, 90°)]/1.5911,$$
$$V_4(R) = [V(R, 0°) - V(R, 90°) - 1.5\,V_2(R)]/0.625. \qquad (3)$$

The analytical fits are compared to the *ab initio* data in Fig. 1(a). As can be seen, the Legendre expansion up to fourth order represents the potential adequately. In Fig. 1(b), the expansion coefficients $V_\lambda(R)$ are plotted as a function of the interparticle separation R. The numerical values of the fit

TABLE I. Parameters for the analytic description of the interaction potential $V(R, \theta)$ according to Eq. (2) at three orientation angles $\theta = 0°, 90°$, and $40°$. See text for details.

	$V(R, 0°)$	$V(R, 90°)$	$V(R, 40°)$
R_0 (Å)	5.8	5.25	5.72
α (Å^{-1})	0.034468	0.034468	0.034468
p_0 (cm^{-1})	-1756256.63	-262228016.79	-267045622.28
p_1 (cm^{-1})	12544629.15	1657141129.59	1703859985.34
p_2 (cm^{-1})	-30069857.17	-4348781360.99	-4518541081.52
p_3 (cm^{-1})	26102330.12	6062945894.88	6372877530.25
p_4 (cm^{-1})	3701700.96	-4733245170.05	-5039612014.95
p_5 (cm^{-1})	-17639551.38	1960411915.99	2117708797.62
p_6 (cm^{-1})	7113286.78	-336249184.65	-369251509.65
C_4 (cm^{-1}Å^4)	-2437572.32	-2869054.88	-2653313.60
C_5 (cm^{-1}Å^5)	-308701429.10	-535117.89	-32081850.31
C_6 (cm^{-1}Å^6)	5063017522.48	-113620695.71	242334325.22
C_7 (cm^{-1}Å^7)	–	–	–
C_8 (cm^{-1}Å^8)	-225693428343.86	-11575979814.12	-22768354089.67

parameters are listed in Table I. The magnitude of the isotropic coefficient V_0 significantly exceeds the one of the anisotropic contributions V_2 and V_4 indicating that the potential is dominated by the strong polarizability of the multi-electron atomic partner, as can be expected from a nonpolar molecular ion interacting with a neutral atom. From this finding, one can already expect elastic processes to dominate over inelastic ones in the present system. Moreover, the repulsive part of the $V_2(R)$ curve effectively shields large parts of the nonvanishing sections of the $V_4(R)$ potential so that it can be expected that the major inelastic processes will involve changes of two units of rotational angular momentum, i.e., $\Delta N = \pm 2$. In this work, N denotes the rotational quantum number of N$_2^+$, j is the quantum number of the total molecular angular momentum without nuclear spin, and J is the quantum number of the total angular momentum of the collision system (excluding nuclear spin).

B. Multichannel quantum scattering calculations

To obtain rotationally inelastic state-to-state integral scattering cross sections (ICS), we employed the ASPIN quantum-scattering code described in Ref. [28]. In the scattering calculations, the atom was treated as a structureless particle while the molecule was incorporated as a rigid rotor with singlet or doublet electron spin.

The integration of the scattering equations for collision energies up to $E_{coll}/k_B = 1100$ K extended out to $R = 220$ Å using a total of 3000 steps. The maximum number of the total angular-momentum quantum number used in the calculations was $J_{max} = 350$, while the maximum number of rotational channels employed was 23. For calculations at low collision energies up to $E_{coll}/k_B = 70$ mK, the integration of the scattering equations extended out to $R = 15\,000$ Å using a total of 30 000 steps and a maximum total angular-momentum quantum number of $J_{max} = 18$, while the maximum number of rotational channels employed was 23. We expect that the final scattering observables are numerically converged to about 5% of their reported values.

III. RESULTS AND DISCUSSION

ICS for rotationally elastic collisions are reported in Fig. 2. In the results shown in Fig. 2(a), the N$_2^+$ moiety has been treated as a species with pseudosinglet electron spin, i.e., it was treated as a closed-shell system and spin-rotation coupling was neglected. Elastic cross sections are reported for the lowest rotational levels $N = 1, 3, 5, 7$ of the molecular ion up to collision energies of $E_{coll}/k_B = 1100$ K. The computed ICS show a monotonic decrease with increasing collision energy
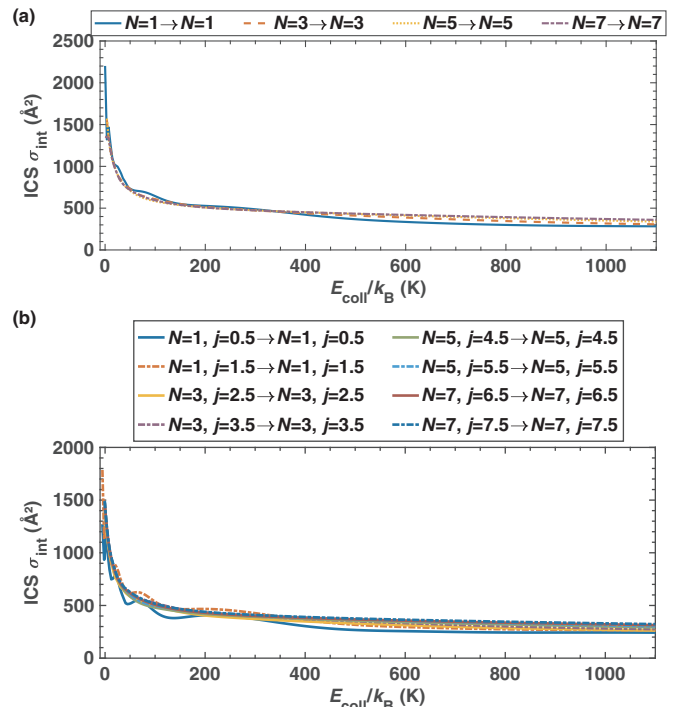

FIG. 2. Computed rotationally elastic ICS for N$_2^+$ + Rb. The molecular ion is treated as a pseudo-singlet-spin species in (a) and as as a doublet-electron-spin species in (b).
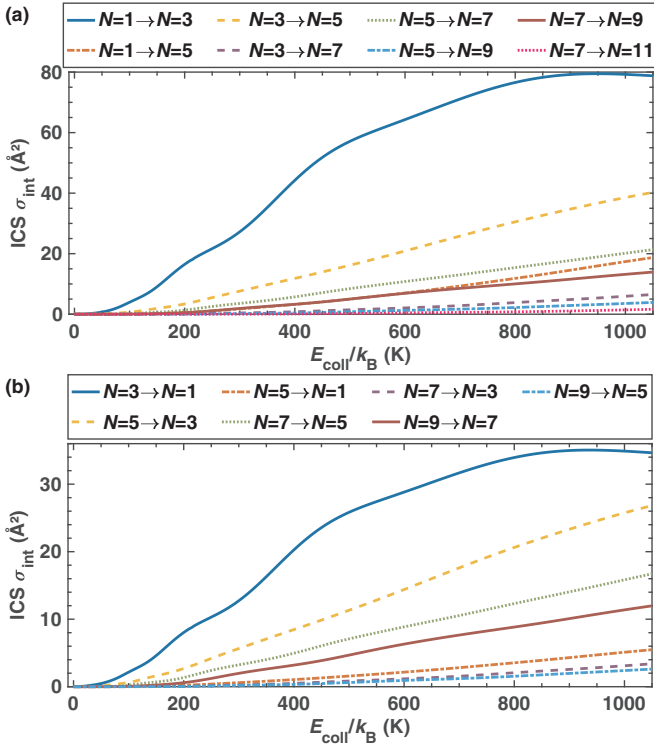
FIG. 3. State-to-state (a) excitation and (b) de-excitation inelastic ICS at collision energies up to 1100 K.

FIG. 4. (a) ICS and (b) rate coefficients at an infinitely small spread of collision velocities and (c) thermal rate coefficients for N_2^+ + Rb elastic collisions in the cold regime.

which is a general behavior often observed in elastic cross sections.

The computational validity of treating N_2^+ as a pseudosinglet rather than a doublet electronic state, the latter requiring the incorporation of spin-rotation coupling in the scattering calculations, is justified by comparing the spin-rotation-resolved elastic cross sections in Fig. 2(b) with the results for the pseudosinglet in Fig. 2(a). The two sets of cross sections agree well with each other and also show a consistent energy dependence. The marginal differences which we see between the two different approximations are essentially negligible for the purpose of the present discussion of purely rotational effects in the scattering. The pseudosinglet approach produces physically reliable values for the quantities of interest here, i.e., rotationally resolved cross sections. We therefore treated the collisional dynamics within the pseudosinglet approximation to reduce the computational costs.

Figures 3(a) and 3(b) show ICS for rotational excitation and de-excitation processes, respectively, for the lowest rotational states in collisions between N_2^+ and Rb in the energy range up to $E_{coll}/k_B = 1100$ K. Note that only state changes with $\Delta N =$ even are allowed assuming the conservation of nuclear-spin symmetry during the collision. We clearly see that over the entire range of collision energies examined, the rotational excitation and de-excitation cross sections show a fairly similar behavior and monotonically increase with collision energy. Both processes exhibit rotationally inelastic cross sections on the order of 1 to 100 Å^2 in the interval $E_{coll}/k_B = 100$–1000 K, which is in line with the expected order of magnitude for such processes in an ionic system, see, e.g., Refs. [29,30] for comparison. The most distinctive
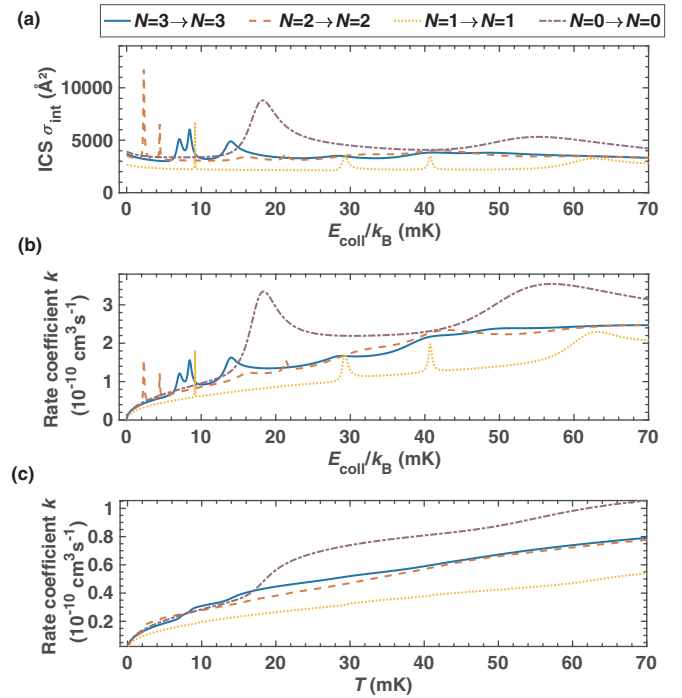
difference lies in transitions involving the lowest rotational states, namely $N = 1$ to 3 and $N = 3$ to 5 and vice versa for which we find a factor of 2 difference between the ICS of the excitation and de-excitation processes. This is reasonable given the different energy gaps exhibited by the two processes. Note also that the cross sections involving changes in the rotational quantum number $\Delta N = \pm 4$ are about an order of magnitude smaller than those associated with $\Delta N = \pm 2$, reflecting the relative magnitude of the $V_{\lambda=2,4}(R)$ coefficients discussed above.

We now turn to examining the cross sections in the regime of collision energies around several tens of millikelvin, which are particularly relevant for hybrid trapping experiments. Figure 4 shows ICS [Fig. 4(a)] and rate constants k [Figs. 4(b) and 4(c)] for rotationally elastic collisions. The rate constants in Fig. 4(b) were calculated assuming an infinitely narrow spread of collision energies in the experiment according to

$$k = \sigma \sqrt{\frac{2E_{coll}}{\mu}}, \qquad (4)$$

where σ is the ICS and μ the reduced mass of the N_2^+ - Rb collision. This situation would approximate an experiment with a high resolution in the collision energy [31,32]. By contrast, Fig. 4(c) shows the thermal rate constants obtained by integrating the cross sections over a Maxwell-Boltzmann distribution of velocities at the relevant temperature. In this energy range, the cross sections exhibit marked variations attributed to scattering resonances. While these resonances also manifest themselves in the rate constants in experiments at high energy resolution [Fig. 4(b)], the narrow features are

almost completely smoothed out in the rate constants under thermal conditions [Fig. 4(c)].

The physical origin of the narrow resonances in the cross sections should be linked to the rather strong ionic interactions which are driving the present dynamics. The resonances observed in Fig. 4 could be shape resonances in which the system is intermittently trapped in a metastable state behind the centrifugal barrier. In addition, the strong coupling between scattering channels due to long-range ion-neutral interactions can also distort the rotational structure of the isolated molecular target creating virtual excitations to excited rotational states (Feshbach resonances) which can be populated during a short time interval during the collisional events. The elucidation of the precise mechanisms causing these resonances would require further theoretical studies.

The narrow widths exhibited by the observed resonances, an indication of their lifetimes, are producing rather limited contributions to the thermal rate coefficients as can be seen in Fig. 4(c). Hence the computational evidence of the occurrence of several narrow resonant features near threshold energies would not translate into observable increases of the overall collision rates over the range of energies of interest studied in thermal experiments. Their observation would therefore require an experiment with a high collision-energy resolution as implied in the rate coefficients calculated in Fig. 4(b) in which the resonance structures are preserved. However, as will be discussed below, the prospects for experimentally observing these inelastic-scattering resonances are in any case limited because of the dominance of charge-exchange processes in the present system.

Generally, the elastic rate coefficients are on the order of 10^{-10} cm^{3}s^{-1} in this energy range, similar to other ionic systems, e.g., H$_2^+$ + He [33], but well below the Langevin rate coefficient $k_L = 3.5 \times 10^{-9}$ cm^{3}s^{-1} for N$_2^+$ + Rb [24].

Figure 5 shows rotational de-excitation cross sections [Fig. 5(a)] and rate coefficients [Figs. 5(b) and 5(c)] across the same range of collision energies. Note that rotational excitations are energetically forbidden at these low collision energies. The cross sections again show pronounced modulations as a function of the collision energy pointing to scattering resonances. Some of the strongest resonances, e.g., the one observed in the $N = 2 \rightarrow N = 0$ channel around $E_{coll}/k_B = 5$ mK, even manifest themselves in the thermal rate constants after thermal averaging in Fig. 5(c). Except at the positions of the strongest resonances observed at high energy resolution, the rotational de-excitation rate coefficients are small with $k < 10^{-11}$ cm^3 s^{-1} in the energy range shown. In particular, they are well below the Langevin limit for this system.

Together with the findings of our previous studies in Refs. [24,26], the present results for inelastic and elastic collision cross sections provide a comprehensive picture of the importance of the different types of collisional processes which can occur in the cold scattering of N$_2^+$ + Rb in their relevant ground states. The fastest process is established to be a nonadiabatic charge transfer in the triplet scattering channel of N$_2^+$ ($X\,^2\Sigma_g^+$) with Rb ($5s\,^2S_{1/2}$), the rate constants for which were found to be on the order of 1.5×10^{-9} cm^{3}s^{-1} at collision energies in the range of tens of mK [24]. This value is only about a factor of 3 smaller than the Langevin
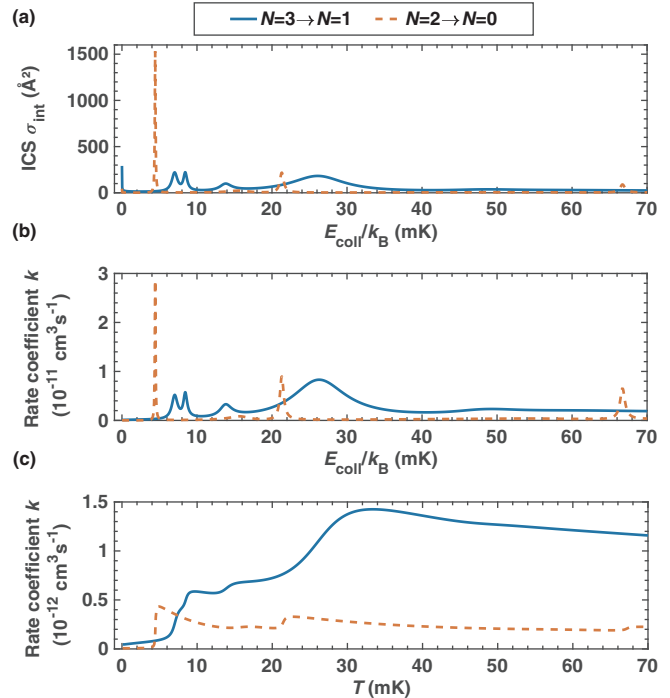

FIG. 5. (a) ICS and (b) rate coefficients at an infinitely small spread of collision velocities and (c) thermal rate coefficients for N$_2^+$ + Rb rotationally inelastic collisions in the cold regime.

limit. Charge exchange thus clearly dominates over elastic and inelastic collisions, the rate coefficients of which were calculated here to be at least one to two orders of magnitude smaller. By contrast, the rates for radiative association to form the N$_2$Rb$^+$ complex were found to be at least five orders of magnitude smaller than the Langevin limit, rendering this process insignificant in experiments. This is in line with the experimental results of Ref. [24] in which charge transfer was indeed found to be the dominant chemical process.

We argue that the dynamical picture which has been found here in N$_2^+$ + Rb can qualitatively be transferred to a wider range of cold collision systems consisting of small molecular ions and alkali atoms with a large difference in the ionization potentials of the two species. In these cases, the possible entrance channels of the collisions will likely be highly excited states of the collision complex in which opportunities may arise for nonadiabatic transitions around curve crossings with other excited states. In this scenario, the charge exchange will likely be the kinetically dominating process, as in N$_2^+$ + Rb and most probably also O$_2^+$ + Rb [24]. Rotationally inelastic collisions, as studied here, and competing reactive processes such as radiative association [26] are likely to exhibit considerably smaller rates. Of course, this does not preclude the possibility of other fast chemical processes which may occur depending on the specific system [23].

IV. CONCLUSION

In this work, we calculated the rate coefficients of elastic and rotationally inelastic collisions in the N$_2^+$ ($X\,^2\Sigma_g^+$) + Rb ($5s\,^2S_{1/2}$) system. Collision cross sections were obtained from

multichannel quantum-scattering calculations performed on *ab initio* potential-energy surfaces of the lowest singlet collision channel. The magnitude and the general trends observed for both the elastic and inelastic cross sections were found to be in line with similar ionic collision systems explored in previous studies. Notably, the elastic and inelastic collision rates were found to be considerably smaller than the charge-transfer reaction rates [24]. Thus, it can be expected that any inelastic processes will be dominated by reactive processes in this system and inelastic collisions will play a small role under typical experimental conditions. Similar scenarios are likely to be found over a wider range of collision systems involving small molecular ions and alkali atoms with a large difference in the ionization energies between the two species.

[1] A. Härter and J. Hecker Denschlag, Contemp. Phys. **55**, 33 (2014).

[2] C. Sias and M. Köhl, *Quantum Gas Experiments* (World Scientific, Singapore, 2014), p. 267.

[3] S. Willitsch, Proc. Int. Sch. Phys. Enrico Fermi **189**, 255 (2015).

[4] S. Willitsch, Adv. Chem. Phys. **162**, 307 (2017).

[5] M. Tomza, K. Jachymski, R. Gerritsma, A. Negretti, T. Calarco, Z. Idziaszek, and P. S. Julienne, Rev. Mod. Phys. **91**, 035001 (2019).

[6] S. Willitsch, Int. Rev. Phys. Chem. **31**, 175 (2012).

[7] A. T. Grier, M. Cetina, F. Oručević, and V. Vuletić, Phys. Rev. Lett. **102**, 223201 (2009).

[8] F. H. J. Hall, M. Aymar, N. Bouloufa-Maafa, O. Dulieu, and S. Willitsch, Phys. Rev. Lett. **107**, 243202 (2011).

[9] W. G. Rellergert, S. T. Sullivan, S. Kotochigova, A. Petrov, K. Chen, S. J. Schowalter, and E. R. Hudson, Phys. Rev. Lett. **107**, 243201 (2011).

[10] D. S. Goodman, I. Sivarajah, J. E. Wells, F. A. Narducci, and W. Smith, Phys. Rev. A **86**, 033408 (2012).

[11] S. Haze, S. Hata, M. Fujinaga, and T. Mukaiyama, Phys. Rev. A **87**, 052715 (2013).

[12] C. Zipkes, S. Palzer, C. Sias, and M. Köhl, Nature **464**, 388 (2010).

[13] S. Schmid, A. Härter, and J. H. Hecker Denschlag, Phys. Rev. Lett. **105**, 133202 (2010).

[14] Z. Meir, T. Sikorsky, R. Ben-shlomi, N. Akerman, Y. Dallal, and R. Ozeri, Phys. Rev. Lett. **117**, 243401 (2016).

[15] J. Joger, H. Fürst, N. Ewald, T. Feldker, M. Tomza, and R. Gerritsma, Phys. Rev. A **96**, 030703(R) (2017).

[16] S. T. Sullivan, W. G. Rellergert, S. Kotochigova, and E. R. Hudson, Phys. Rev. Lett. **109**, 223002 (2012).

[17] H. da Silva, Jr., M. Raoult, M. Aymar, and O. Dulieu, New J. Phys. **17**, 045015 (2015).

[18] L. Ratschbacher, C. Zipkes, C. Sias, and M. Köhl, Nat. Phys. **8**, 649 (2012).

[19] T. Sikorsky, Z. Meir, R. Ben-shlomi, N. Akerman, and R. Ozeri, Nat. Commun. **9**, 920 (2018).

[20] T. Sikorsky, M. Morita, Z. Meir, A. A. Buchachenko, R. Ben-shlomi, N. Akerman, E. Narevicius, T. V. Tscherbul, and R. Ozeri, Phys. Rev. Lett. **121**, 173402 (2018).

[21] F. H. J. Hall and S. Willitsch, Phys. Rev. Lett. **109**, 233202 (2012).

[22] W. G. Rellergert, S. T. Sullivan, S. J. Schowalter, S. Kotochigova, K. Chen, and E. R. Hudson, Nature **495**, 490 (2013).

[23] P. Puri, M. Mills, C. Schneider, I. Simbotin, J. A. Montgomery, R. Côté, A. G. Suits, and E. R. Hudson, Science **357**, 1370 (2017).

[24] A. D. Dörfler, P. Eberle, D. Koner, M. Tomza, M. Meuwly, and S. Willitsch, Nat. Commun. **10**, 5429 (2019).

[25] P. Puri, M. Mills, I. Simbotin, J. A. Montgomery, R. Côté, C. Schneider, A. G. Suits, and E. R. Hudson, Nat. Chem. **11**, 615 (2019).

[26] F. A. Gianturco, A. D. Dörfler, S. Willitsch, E. Yurtsever, T. González-Lezana, and P. Villarreal, Phys. Chem. Chem. Phys. **21**, 8342 (2019).

[27] W. D. Hall and J. C. Zorn, Phys. Rev. A **10**, 1141 (1974).

[28] D. López-Durán, E. Bodo, and F. A. Gianturco, Comput. Phys. Commun. **179**, 821 (2008).

[29] L. González-Sánchez, R. Wester, and F. A. Gianturco, Phys. Rev. A **98**, 053423 (2018).

[30] M. H. Vera, E. Yurtsever, R. Wester, and F. A. Gianturco, J. Chem. Phys **148**, 184305 (2018).

[31] P. Eberle, A. D. Dörfler, C. von Planta, K. Ravi, and S. Willitsch, Chem. Phys. Chem. **17**, 3769 (2016).

[32] P. Puri, M. Mills, E. P. West, C. Schneider, and E. R. Hudson, Rev. Sci. Instr. **89**, 083112 (2018).

[33] S. Schiller, I. Kortunov, M. H. Vera, F. Gianturco, and H. da Silva, Jr., Phys. Rev. A **95**, 043411 (2017).